ELSEVIER

Thermochimica Acta 382 (2002) 99–107

thermochimica acta

www.elsevier.com/locate/tca

Experimental verification of calculated radiation-induced heat conduction effects in the water absorbed dose calorimeter

A. Krauss*

Physikalisch-Technische Bundesanstalt (PTB), Fachlabor 6.22, Bundesallee 100, D-38116 Braunschweig, Germany

Received 20 April 2001; accepted 15 May 2001

Abstract

Water absorbed dose calorimeters will be used as PTB standards for the dosimetry in radiation therapy. In this investigation, heat conduction effects in the calorimeter due to the irradiation of the non-water materials of the plane-parallel detector are investigated experimentally and by model calculations. It is shown that the effects during ^{60}Co-γ-irradiation can be adequately described by finite-element simulations and that corresponding corrections in the order of 0.2% result for the typical operating mode of the calorimeter. Correction factors k_C are determined for a variety of different irradiation conditions.

Keywords: Heat conduction; Finite-element method; Plane-parallel detector cylinder; Correction factor (k_C); Water absorbed dose calorimeter

1. Introduction

At Physikalisch-Technische Bundesanstalt (PTB), a water absorbed dose calorimeter [1,2] will shortly be established as a primary standard realizing the unit gray (Gy) for water absorbed dose, D_W, at ^{60}Co-γ-radiation. The quantity water absorbed dose is the measurand in the dosimetry for radiation therapy and is defined as the differential quotient of $d\varepsilon/dm$, where $d\varepsilon$ is the mean energy imparted by radiation to water of the mass dm at the point of measurement. The calorimetric determination of this quantity basically consists in the measurement of the radiation-induced temperature rise, $\Delta\vartheta$, at a point in a water phantom multiplied by the specific heat capacity, c_p, of water:

$$D_W = \Delta\vartheta c_p \frac{1}{1-h} \prod k_i \quad (1)$$

The parameter h allows for the so-called ''heat defect'', which is the relative difference between the energy imparted to water and the energy occurring as heat [3,4]. The $\prod k_i$ is the product of several correction factors, for example for the perturbation of the radiation field by the caloric detector or for the heat conduction effects inside the calorimeter. The latter is denoted as k_C [5,6]. The heat conduction effects are mainly caused by the irradiation of the non-water materials (e.g. glass) of the caloric detector. The values of the specific heat capacities and of the radiation interaction coefficients of these materials deviate from those of water, leading to a higher temperature increase in the non-water materials. These effects can either be kept negligibly small by constructional measures or, alternatively, must be corrected by heat conduction calculations. However, this requires a caloric detector of well-defined geometry.

Different types of detectors have been developed at PTB [7–9]. For the primary standard water calorimeter

* Tel.: +49-531-5926432; fax: +49-531-5926405.
E-mail address: achim.krauss@ptb.de (A. Krauss).

0040-6031/02/$ – see front matter
PII: S0040-6031(01)00743-2

a sealed detector will be used, consisting of a water-filled glass cylinder in which two thin glass pipettes, each containing a thermistor sensor, are mounted opposite each other. The final cylinder design, shown in Fig. 1, is a plane-parallel glass cylinder with the cylinder axis parallel to the beam axis [10]. This detector cylinder offers the advantage that it is manufactured very precisely, with flat front and rear walls of very small and homogenous wall thickness. The geometry of the caloric detector can therefore be adequately modeled within a finite-element computer program, allowing verification of

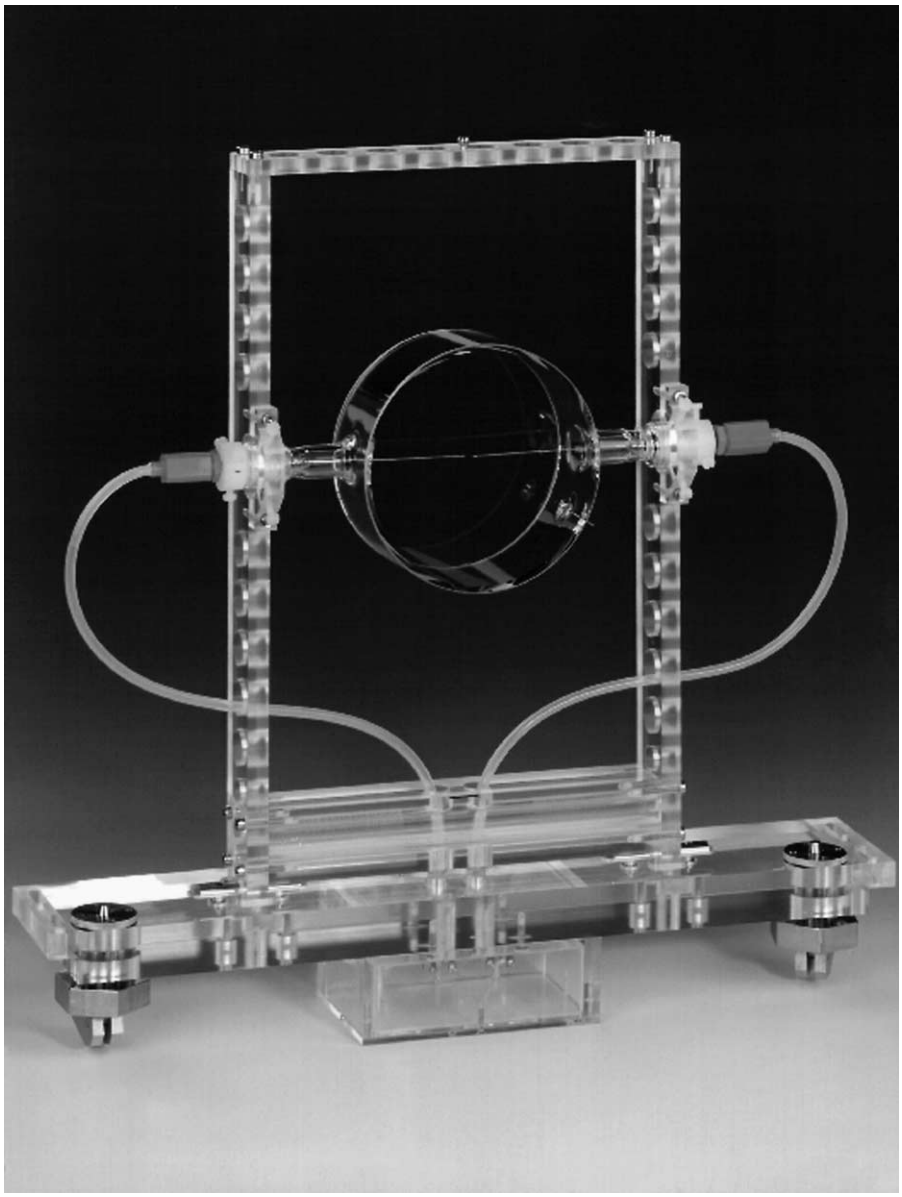

Fig. 1. Picture of the plane-parallel detector of the water absorbed dose calorimeter, showing the glass cylinder with the thermistor pipettes in a PMMA mount. During irradiation, the ^{60}Co-γ-radiation field is directed perpendicularly towards the thin flat walls of the cylinder.

the results calculated for the heat conduction effects by comparison with the corresponding experimental data.

In this paper, for a specific irradiation condition, the results of finite-element heat conduction calculations of the irradiation of the detector walls and the thermistor sensors are compared with the results of caloric measurements performed with ^{60}Co-γ-radiation. In addition, the corresponding correction factors, k_C, to be applied to Eq. (1) are determined for a variety of different irradiation conditions.

2. Materials and methods

2.1. Calorimeter

The details of the construction and the performance of the water absorbed dose calorimeter have been described previously [8]. Essentially, it consists of a 30 cm × 30 cm × 30 cm water-filled cubic container made of 1 cm thick polymethylmethacrylate (PMMA), which is thermally isolated by an 8 cm thick layer of polystyrene. This calorimeter box is placed inside a second, larger container in which active temperature stabilization is achieved by a forced stream of temperature-controlled air. To avoid convection in the water, the calorimeter is operated at a water temperature of 4 °C [7].

The calorimetric detector is placed into the water phantom on a PMMA mount at a water depth of 5 cm in relation to the PMMA radiation entrance window 0.3 cm in thickness. The plane-parallel glass cylinder of the detector used for this investigation has an outer diameter of 95 mm, with a wall thickness of 2.5 mm and an outer length of 41.5 mm, the front and rear walls being 0.75 mm in thickness. Possible variations of the wall thickness are specified by the manufacturer to be 0.05 and 0.1 mm for the flat wall and the cylinder wall, respectively. The variation of the outer cylinder dimensions has been determined to be 0.2 and 0.1 mm for the diameter and the length, respectively. Two conically shaped glass pipettes with an outer diameter at the tip of 0.50 mm, containing a 0.25 mm diameter thermistor embedded in glass over a length of about 1.5 mm, are mounted opposite each other at a distance of about 10 mm inside the glass cylinder. The position of the thermistor glass pipettes inside the cylinder is determined by an optical method with an uncertainty of about 0.05 mm.

During irradiation in the extended horizontally directed ^{60}Co-γ-radiation field, the resulting temperature increase at the point of measurement is determined from the output of a dc-powered resistance bridge.

2.2. Heat transport calculations

For the calculation of the radiation-induced heat transport effects inside the water phantom, a three-dimensional model of the phantom, including the sealed detector has been developed within a finite-element program (ANSYS 5.6), taking into account the nominal dimensions of the cylinder. In Fig. 2, a schematic representation of the detector model is given, showing the glass cylinder (without front and rear walls) and the more massive parts of the glass pipettes. For the model shown, the element density, especially at the tip of the glass pipettes, could not be chosen high enough for a reliable calculation of the combined effect of the irradiation of the cylinder walls and the pipettes. The model presented was, therefore, separated into two independent parts in order to perform the transient calculation of the irradiation of the

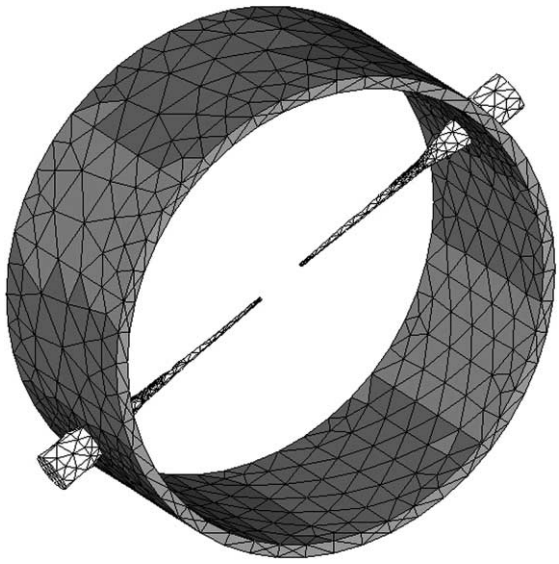

Fig. 2. Three-dimensional detector model used for the finite-element calculations. The flat front and rear walls of the glass cylinder are not shown.

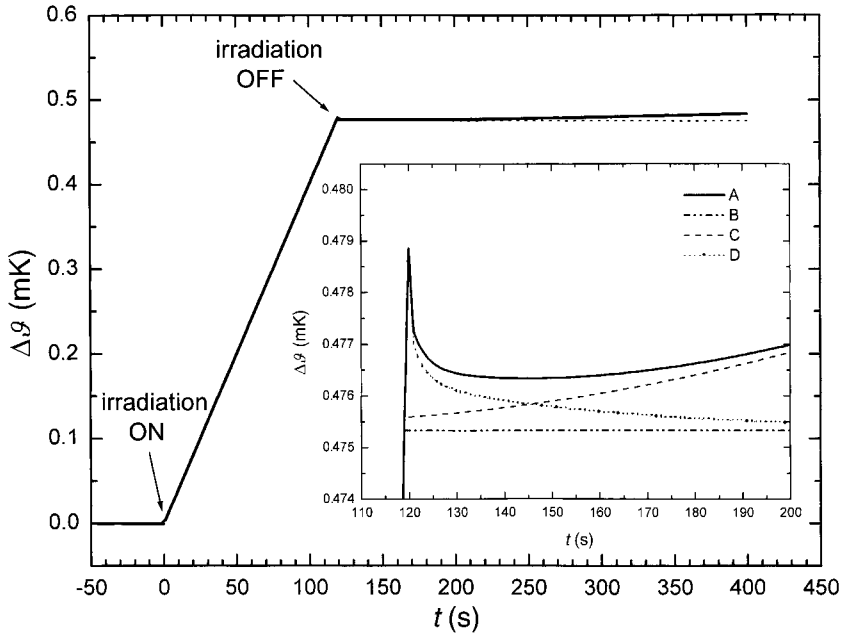

Fig. 3. Calculated temperature signal of the calorimeter during and after ^{60}Co-γ-irradiation (irradiation time: 120 s, dose rate: 1 Gy/min). The inset shows the principal development of the post-irradiation drift curve with time, including the overall heat conduction effects (A), the undisturbed temperature signal (B), the "wall effect" (C), and the "thermistor effect" (D).

detector walls ("wall effect") and of the glass pipettes including the embedded thermistor ("thermistor effect"), assuming that the "wall effect" and "thermistor effect" superimpose without disturbance. In Fig. 3, the principal development of both effects, and of the combined effect, with time is shown for an irradiation time of 120 s. As the "thermistor effect" exponentially decreases within about 10 s after the end of the irradiation, the "wall effect" smoothly increases and dominates the post-irradiation drift curve for longer time periods.

Table 1 summarizes the material properties used for the finite-element calculations. The manufacturer of the thermistors does not state the density and the thermal properties of the thermistor material. Therefore, these parameters were previously estimated by model calculation as a possible set of coupled parameters which adequately describe the measured time response of a change in electrical power consumption of a thermistor glass pipette in water [9]. However, the results of the heat conduction calculations depend more strongly on the wall thickness and geometric parameters of the non-water materials than on their thermal parameters.

The radiation-induced temperature increase in different materials in the same radiation field directly depends on the mass energy absorption coefficient. The corresponding ratio between glass and water for ^{60}Co-γ-radiation was derived by Monte Carlo calculation to be 0.898. This ratio was also taken for the relative energy deposition in the thermistor material.

Model calculations were performed for conditions identical to those applied in the caloric experiments

Table 1
Density (ρ), thermal conductivity (k), and specific heat capacity (c_p) of the materials used for the model calculations

	ρ (kg m^{-3})	k (J s^{-1} m^{-1} K^{-1})	c_p (J kg^{-1} K^{-1})
Water [13]	1000	0.568	4206.8
Glass [13,14]	2230	1.10	750
Thermistor [9]	4000[a]	3.5[a]	250[a]

[a] The manufacturer of the thermistors does not state the density and the thermal properties of the thermistor material. Therefore, these parameters were previously estimated by model calculation as a possible set of coupled parameters which adequately describe the measured time response of a change in electrical power consumption of a thermistor glass pipette in water.

regarding radiation time and time between successive irradiations. As heat conduction effects caused by the initial radiation-induced temperature, profile in water (corresponding to the depth dose profile) were found to be negligible in a previous investigation [11], it was assumed that the dose profile inside the calorimeter was uniform during irradiation. It was furthermore assumed that the radiation-induced temperature increase in the water outside the detector cylinder was by 3.5% higher than in the water inside the cylinder. This assumption was based on experimental results and on theoretical considerations about the radiation chemistry of water contaminated by small amounts of organic impurities [4], leading to an exothermal heat defect of about that value. The presence of such impurities could be expected because the water in the PMMA phantom is more or less open to the environment.

2.3. Experiments

All measurements with the water absorbed dose calorimeter were performed at a water temperature of 4 °C. The distance between the surface of the water phantom and the ^{60}Co-γ-source was 1 m, resulting in a dose rate of about 0.35 Gy/min at the point of measurement. The beam diameter of the horizontally directed radiation field at the phantom surface was 259 and 207 mm with respect to the 50 and 95% dose rate value, respectively.

For the investigation presented here, two different kinds of experiments were performed. In the first experiment, only a single irradiation of 120 or 240 s, followed by a longer post-irradiation drift period of up to 300 s, was applied, before the water in the phantom was newly mixed in order to remove all temperature gradients inside. Then the next irradiation was started. These measurements served as a direct verification of the calculated post-irradiation drift curves of the calorimeter over a time period of several minutes.

In the second type of experiment, a sequence of eight irradiations was performed without mixing of the water. This method of operating the calorimeter is the typical way followed for the determination of the water absorbed dose. Both, the irradiation time and the post-irradiation drift period, were 120 s, the latter being the pre-irradiation drift period of the next irradiation. After eight irradiations the water was newly mixed and another sequence of eight measurements was started. In this case, and for different irradiation times and/or drift periods as well, calculated correction factors, k_C, for the overall heat conduction effects must be applied to every single measurement or to the mean value of a sequence of irradiations.

3. Results and discussion

3.1. Post-irradiation drift curves

Figs. 4 and 5 present the experimental results and the results of the computations for an irradiation time of 120 and 240 s, respectively. For each case, the mean voltage signal of 40 caloric measurements after the end of the irradiation has been plotted as a function of time. Before the signals were summarized, the gradients of the pre-irradiation drift curves of the single measurements were normalized to zero. The results of the model calculations have been fitted to the experimental data over a post-irradiation drift interval of 240 s. For both irradiation times agreement between experimental data and calculation is good in respect of the time evolution of the post-irradiation drift curves, with the exception of the first 2 or 3 s after the end of irradiation. Generally, this is taken as a proof of the validity of the finite-element heat conduction calculations and of the possibility of adequately correcting the radiation-induced heat conduction effects on the basis of model calculations.

If the detector dimensions are varied within their uncertainties in the finite-element model calculations, slight changes of the shape of the post-irradiation drift curves occur, especially for longer time periods after the end of an irradiation. Similar changes occur if a different heat defect for the water outside the detector cylinder is assumed (Section 3.3).

3.2. "Thermistor effect"

As can be gathered from the post-irradiation drift curves of Fig. 4 or Fig. 5, the amplitude of the calculated "thermistor effect" just at the end of the irradiation is much smaller than the measured amplitude. However, this is of no significance for the results of caloric measurements, as this effect rapidly vanishes and the caloric results are determined by

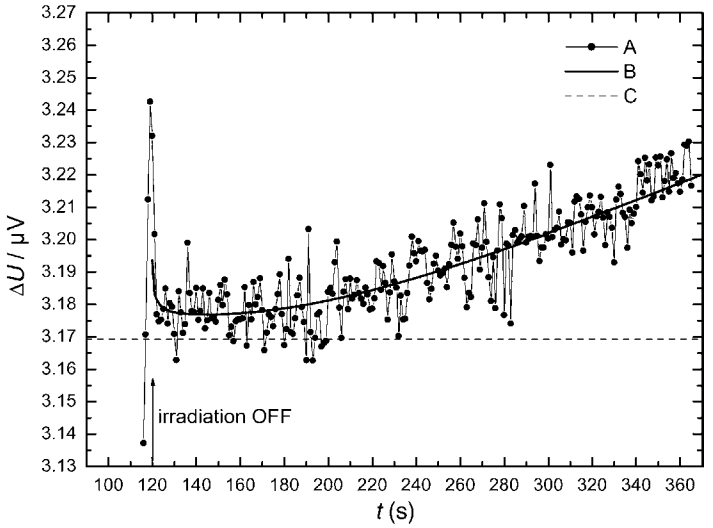

Fig. 4. Experimental post-irradiation drift curve for an irradiation time of 120 s. The figure shows the mean voltage signal of 40 measurements (A); a voltage difference of 0.1 μV corresponds to a change in temperature by about 6 μK. The calculated heat conduction effect due to irradiation of the thermistors and the detector walls has been fitted to the experimental data over a time interval of 240 s (B). The undisturbed post-irradiation drift is given by (C).

linear extrapolation of post-period time intervals starting 10 s after the end of irradiation (Section 3.3).

A possible reason for the discrepancy between the measured and calculated amplitude of the ''thermistor effect'' could be, that the thermal ''thermistor effect'' in the experiments is superimposed by an additional non-thermal effect (with faster response) due to the formation of electron-hole pairs in the thermistor

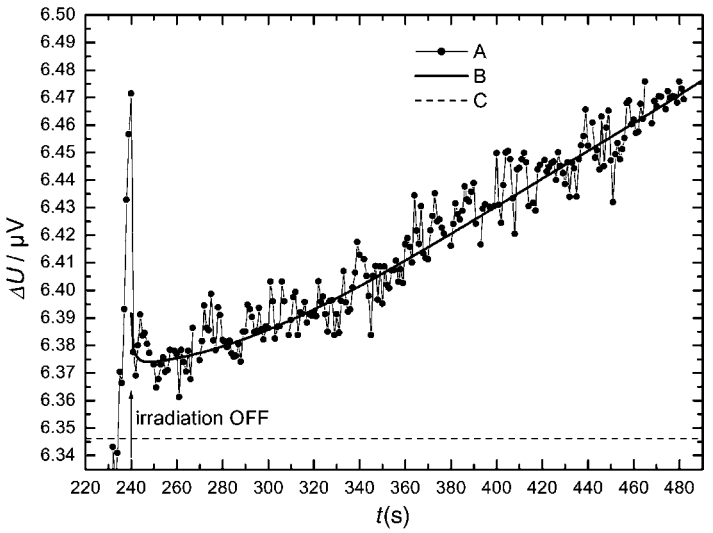

Fig. 5. Experimental post-irradiation drift curve for an irradiation time of 240 s. The figure shows the mean voltage signal of 40 measurements (A); a voltage difference of 0.1 μV corresponds to a change in temperature by about 6 μK. The calculated heat conduction effect due to irradiation of the thermistors and the detector walls has been fitted to the experimental data over a time interval of 240 s (B). The undisturbed post-irradiation drift is given by (C).

semiconductor material. If the external dc voltage applied to the thermistors (about 0.4 V) can separate these charges before recombination takes place, then an additional radiation-induced current will be detectable which vanishes rapidly when irradiation is stopped. A rough estimation leads to an additional current during irradiation in the order of 10 pA needed to explain the additional amplitude of the ''thermistor effect'' seen in the experiments. This is well within the order of magnitude of what can be estimated for an ''ionization'' current, considering the volume and material of the thermistor in comparison with an air-filled ionization chamber. In a previous investigation on the transient thermistor response to radiation, using thermistors within an ac-powered resistance bridge, no such effects could be detected [12].

3.3. Correction factor k_C

The result of a caloric measurement is determined from the linear extrapolation of the pre- and post-irradiation drift curves to the mid-run position. The correction factor k_C is the ratio of such a caloric result without and with influence of the heat conduction effects, and it is determined from the corresponding linear fits to the calculated pre- and post-irradiation drift curves. Table 2 summarizes the pre- and post-irradiation drift intervals chosen for different irradiation times. For the results presented in the following, the post-irradiation time interval chosen to analyze a measurement or calculation starts 10 s after the end of an irradiation. At this time the calculated relative influence of the sharply decreasing ''thermistor effect'' is reduced to about 0.1%.

Table 2
Time intervals (s) chosen for linear fitting of the pre- and post-irradiation drift curves for different irradiation times

Irradiation time (s)	Pre-irradiation time interval (s)	Post-irradiation time interval (s)
60	[−90, 0]	[10, 90]
90	[−120, 0]	[10, 120]
120	[−120, 0]	[10, 120]
240	[−180, 0]	[10, 180]

In the case of a sequence of several irradiations, the pre- and post-irradiation drift curves of a later irradiation are superimposed by the heat conduction effects of the former irradiations, leading to a dependence of the caloric results on the number of measurements. Fig. 6 presents mean values and their standard uncertainties for caloric measurements performed in a

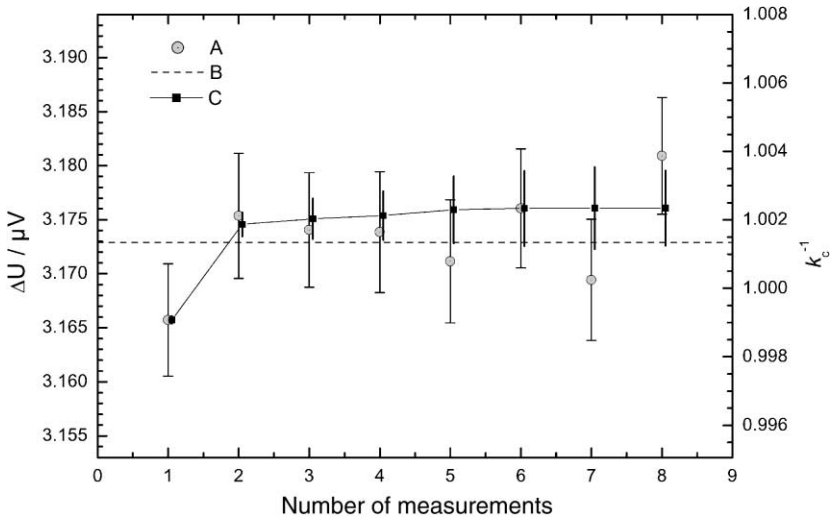

Fig. 6. Results of caloric measurements (irradiation time: 120 s, pre- and post-irradiation drift: 120 s) in dependence on the number of irradiations after the last mixing of the water inside the calorimeter (A); (B) is the overall experimental mean value. The inverse of the calculated correction factor k_C, normalized to the first measurement, is given as (C). For the experimental results, the standard uncertainties of the mean values are given as error bars. The error bars for the calculated results have been derived from the standard uncertainties of the linear fit parameters of the pre- and post-irradiation drift curve fits.

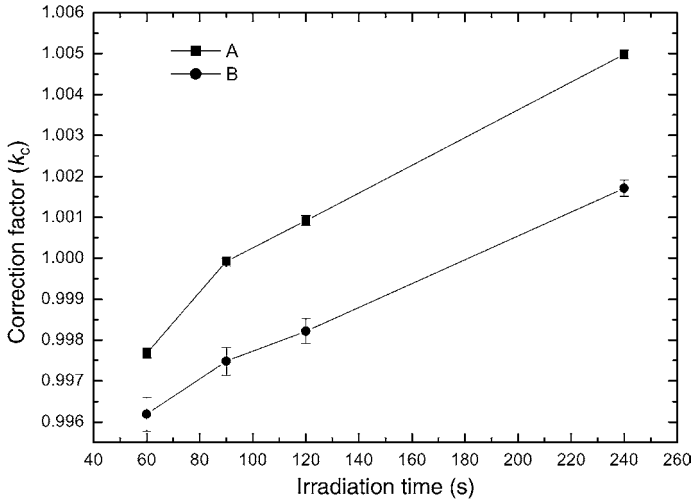

Fig. 7. Calculated heat conduction correction factors for different irradiation times between 60 and 240 s, showing the difference between the results of the first measurement (A); and of the mean of a sequence of eight measurements (B). The chosen pre- and post-irradiation drift intervals are given for every irradiation condition. The error bars have been derived from the standard uncertainties of the linear fit parameters of the pre- and post-irradiation drift curve fits.

sequence of eight irradiations (irradiation time: 120 s, pre- and post-period time: 120 s), showing a major change between the first and the second irradiation. The inverse of the corresponding calculated correction factor k_C, normalized to the first measurement, is also shown in Fig. 6. For the calculated values, the standard uncertainties arising from the uncertainties of the linear fit parameters are given. Reasonable agreement between measurement and calculation is achieved. However, for the last irradiations, the influence of heat conduction effects, which had not been taken into account in the model calculations, had to be expected, due, for example, to the irradiation of the detector mount or of the more massive electrical connectors of the thermistor pipettes (Fig. 1).

Fig. 7 shows calculated correction factors k_C for different irradiation times between 60 and 240 s for a certain set of time intervals for the pre- and post-irradiation drift curves. For an irradiation time of 120 s, k_C is 1.001 for the first measurement and 0.998 for the mean of a sequence of eight measurements. The standard uncertainties given in Fig. 7 again result from the linear fitting procedures. For the case of a sequence of eight irradiations of 120 s, the relative standard uncertainty of k_C therefore is in the order of 0.03%.

Heat conduction calculations performed for detector dimensions varying within their uncertainties lead to relative differences of the correction factors k_C in the order of 0.05% for an irradiation of 240 s and of less than 0.03% for irradiation times between 60 and 120 s. The influence of the assumed heat defect value for the water outside the detector is also small at these irradiation times, the relative differences for k_C being less than 0.02%. For an irradiation time of 240 s, however, k_C is smaller by about 0.09% if the heat defect is neglected. If similar uncertainties are taken into account, which result from the assumptions made within the finite-element calculations, it is concluded that the relative combined standard uncertainty of the calculated correction factor for an irradiation time of 120 s is about 0.06%.

4. Conclusions

Heat conduction effects in the water absorbed dose calorimeter due to the ^{60}Co-γ-irradiation of the non-water materials of the plane-parallel detector were investigated experimentally and by model calculations. It is shown that the results of model calculations agree with the corresponding experimental results. Based on this investigation, correction factors (k_C) can be calculated for a variety of different irradiation conditions. Relative corrections for the heat conduc-

tion effects in the order of 0.2% result for the typical operating mode of the calorimeter, for an irradiation time of 120 s. As the water absorbed dose calorimeter is also applicable in high-energy electron radiation fields, corresponding heat conduction simulations for this case will be performed in the near future. The depth dose profile and the lateral beam profile of the irradiation will then be taken into account as well.

References

[1] S.R. Domen, J. Res. Nat. Bur. Stand. 87 (3) (1982) 211–235.
[2] C.K. Ross, N.V. Klassen, Phys. Med. Biol. 41 (1996) 1–29.
[3] A. Krauss, M. Roos, Thermochim. Acta 229 (1993) 125–132.
[4] N.V. Klassen, C.K. Ross, Radiat. Phys. Chem. 38 (1) (1991) 95–104.
[5] H. Palmans, in: Proceedings of the NPL Workshop on Recent Advances in Calorimetric Absorbed Dose Standards, NPL Report CIRM 42, 2000, pp. 74–84.
[6] J. Seuntjens, H. Palmans, Phys. Med. Biol. 44 (1999) 627–646.
[7] S.R. Domen, A. Krauss, M. Roos, Thermochim. Acta 187 (1991) 225–233.
[8] A. Krauss, M. Roos, Thermochim. Acta 310 (1998) 53–60.
[9] A. Krauss, M. Roos, Thermochim. Acta 337 (1999) 45–49.
[10] A.R. DuSautoy, A.J. Williams, K.E. Rosser, S.J. Gnaniah, Med. Biol. Eng. Comput. 35 (Suppl. Part 2) (1997) 1091.
[11] M. Roos, Thermochim. Acta 119 (1987) 81–93.
[12] C.K. Ross, J.P. Seuntjens, N.V. Klassen, K.R. Shortt, in: Proceedings of the NPL Workshop on Recent Advances in Calorimetric Absorbed Dose Standards, NPL Report CIRM 42, 2000, pp. 90–102.
[13] Kohlrausch, Praktische Physik, 24th Edition, B.G. Teubner, Stuttgart, 1996.
[14] Handbook of Chemistry and Physics, 78th Edition, CRC Press, New York, 1996.